Heliyon 5 (2019) e02388

Contents lists available at ScienceDirect

Heliyon

journal homepage: www.heliyon.com

Heliyon

Study of the low-temperature plasma treatment effect on the structure, physical and chemical surface characteristics of 40X13 steel

Boris Brzhozovskii, Marina Brovkova, Irina Gots, Helena Zinina, Vladimir Martynov *

Institute of Machines Science named after A.A. Blagonravov of the Russian Academy of Sciences, 4 Maly Kharitonyevsky Pereulok, Moscow, 101990, Russia

ARTICLE INFO

Keywords:
Materials science
Surface passivation
Corrosion resistance
Stainless steel
Low-temperature plasma treatment

ABSTRACT

The article examines the influence of a new unparalleled method of low-temperature plasma treatment at 300 Pa pressure on the structure, properties and corrosion resistance of 40X13 steel. Experiments proved that increase in corrosion resistance is achieved by means of innhibition of oxygen depolarization, changes in its limiting stages and, as a consequence, decreased formation rates of oxides and hydroxides of iron and chromium.

1. Introduction

40X13 steel (analogues of which are 420 steel in the USA, 1.4031 steel in Germany, 4C13 steel in China) is widely used in manufacturing products of various purpose (cutting, surgical and special tools, springs, carburetor needles, compressor valve plates, bearings, fasteners, shafts, elastic elements, etc.) operating under various conditions, including extreme aggressive environments that accelerate chemical processes on the surface. In this regard, increasing the operational reliability of such products, in terms of corrosion resistance in particular, is a challenging issue. Various approaches are used in order to solve it, for instance, chemical or electrochemical methods that apply protective coatings to the working surfaces of products. This leads to the transition of the product surface into an inactive (passive) state due to the formation of oxide film and adsorption or phase layers which form a tight, almost impermeable barrier which inhibits or completely stops corrosion.

For passivation, solutions based on oxidizing agents capable of forming hardly soluble compounds (chromates, molybdates, nitrates in alkaline medium, etc.) are used. To avoid oxygen and moisture on the surface, bluing, application of paint, polymer coatings and enameling are used.

The main problem of increasing the corrosion resistance through protective coating application is how to ensure a long-term bond of the coating with the substrate. In this regard, alternative methods are being developed that allow not to apply but to form a coating directly in the product surface layer using various ways, in particular, low-temperature plasma during nitriding or carbonitriding [1, 2, 3, 4]. This allows you to increase the surface layer hardness and thickness, which ensures the best corrosion properties of the product. However, it takes a long time (15 h). We present here an original method to affect the surface of a product with a low-temperature combined discharge plasma under reduced pressure for no more than 15 min [5]. Such plasma is generated in a special process unit directly around the workpiece surface when superhigh-frequency electromagnetic and electrostatic fields are superimposed. The electrostatic field keeps the electrons arising as a result of ionization by the electromagnetic field near the product surface, which contributes to the release in the product of a bigger amount of heat necessary for melting of a thin surface layer. As a result, a "coating-sublayer" structure (Fig. 1) consisting of 30 ... 200 nm particles (nanoclusters) and <10 nm particles (amorphous binder) is formed in it [6, 7]. Microasperities are melted ensuring the filling of micro scratches and small scratches, which improvement of surface roughness (Fig. 2). While in operation, this can contribute to increased corrosion resistance. In order to confirm this conclusion, tests of 40X13 steel before and after low-temperature plasma treatment for corrosion resistance were carried out. The choice of this particular type of testing is due to the fact that, unlike the abrasion resistance tests, it requires less technical preparation and less time while ensuring the required validity and significance of the results obtained.

2. Materials and methods

2.1. Specimen preparation

Tests for corrosion resistance were carried out on 2 machined samples

* Corresponding author.
E-mail address: v_martynov@mail.ru (V. Martynov).

https://doi.org/10.1016/j.heliyon.2019.e02388
Received 22 May 2019; Received in revised form 15 July 2019; Accepted 27 August 2019

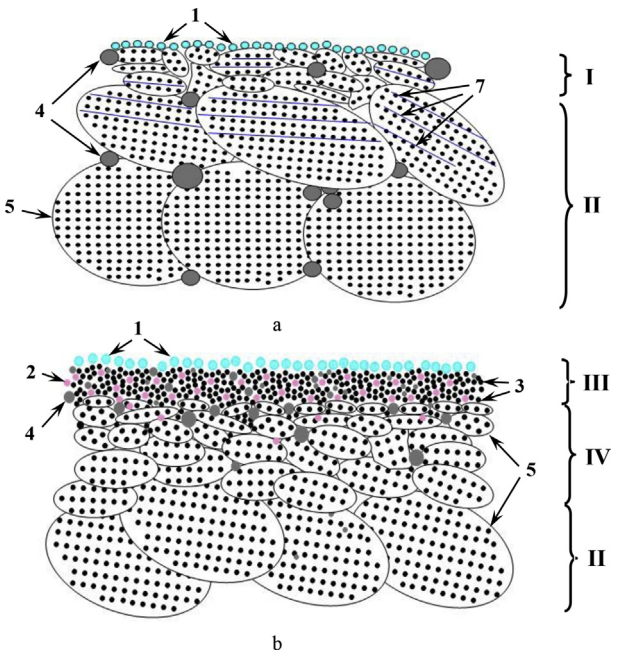

Fig. 1. Diagrams of the original (a) and modified (b) surface layer: I – surface layer, II – matrix, III – coating, IV – sublayer, 1 – adsorbed atoms and a layer of oxides, 2 – interstitial atoms, 3 – ferrite, 4 – carbide grains, 5 – ferritic grains, 6 – dislocations.

of 40X13 steel (⌀8 × 50 mm and mass 33.6 g) with a surface roughness of 3.2 μm at Ra scale: reference and treated in low-temperature plasma. Pre-cleaned and degreased in hot trichlorethylene sample was installed in the mandrel fixed in the holder. The surface of the mandrel and part of the sample surface that was not subject to treatment were isolated by two layers of thin fluoroplastic tape (Fig. 3, position 1), and the mandrel was located in the process chamber developed by the authors of the technological unit [5] according to the coordinates corresponding to the type and size of the sample (position 2). The chamber was then sealed and evacuated to the maximum pressure of 10 Pa (position 3), after which the process gas (N_2, position 4) was inflated to achieve pressure figures of 300 Pa corresponding to the minimum strength of the breakdown fields [8] in the continuous mode of magnetron generation. Then the power supply providing 150 volt potential of the electrostatic field to the sample and the power supply unit of the microwave energy generator were turned on. A smooth adjustment of the magnetron anode current supplied microwave power of 30 W to the chamber (position 6). The treatment lasted 8 min (position 7). After the treatment, the sample was cooled in a protective environment (position 8); it was removed from the holder after depressurization of the working chamber.

2.2. Procedure of corrosion tests

The preparation of sample surfaces prior to testing included mechanical grinding, stabilization in a soap solution, washing, degreasing with ethanol, and drying.

The tests were carried out using gravimetric method (in accordance with GOST 9.909–86 [9]) and consisted in determining corrosion losses from the weight measurements of samples before immersion in 3% NaCl solution for 24 h, as well as the rate of corrosion product formation (v) according to the formula:

$$v = \Delta m/S \times t, \quad (1)$$

where Δm – weight decrease (increase); S – surface area; t – time.

2.3. Equipment used

A study of the morphology and chemical composition of the sample surface layer on an analytic complex based on the TESCAN MIRA\\LMU scanning electron microscope and the INCAPentaFETx3 X-ray sensor

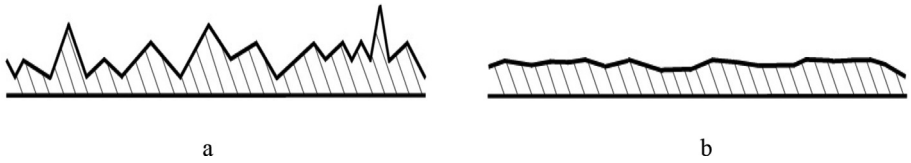

Fig. 2. Surface microrelief: a – original; b – formed as a result of low-temperature plasma treatment.

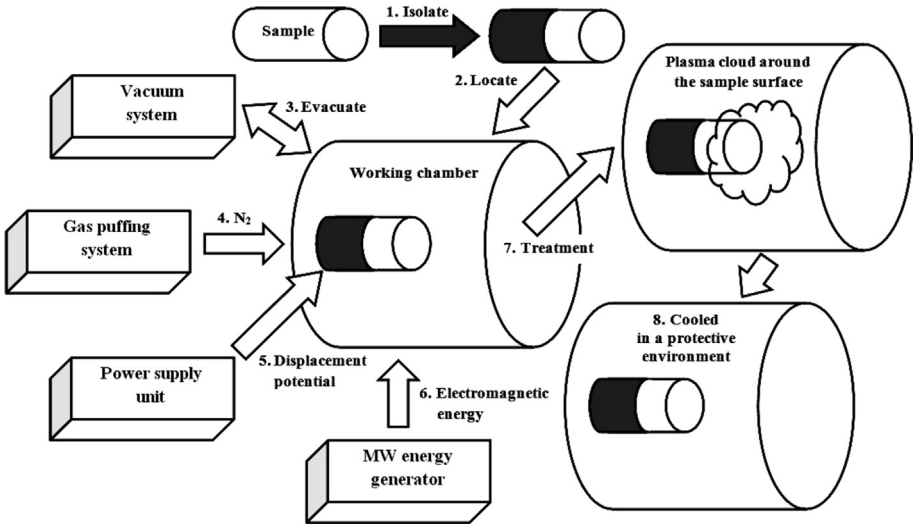

Fig. 3. The general diagram of the low-temperature plasma treatment.

included in its composition, OXFORD Instruments.

The microhardness of the samples was determined on a PMT-3 microhardness meter using the Vickers method and weights of 20 ... 200 g. With each load, 4 measurements were performed; the uniformity of measured values was estimated by calculating the variation coefficient, and in the case of a positive result, the values were averaged, which allowed to obtain a statistically reliable microhardness distribution in the depth of the surface layer.

The measurements were carried out before and after the corrosion tests on Renishaw inVia microscope (Renishaw, UK) using a laser with 532 nm wavelength and 3 mWpower on the sample (if necessary, the power was increased to 30 mW, unless there was an obvious change in the spectra). The spectra were recorded in the SynchroScan mode (scanning by a 1800 lines/mm grid rotation) with time to a point of 10 s. Approximation of the peaks was carried out in Chemometrics package of the standard WiRE v.4.2 software. In addition, extra processing of the obtained spectra was performed including their smoothing by the moving average of seven points, differentiation and scaling.

3. Results and discussion

3.1. The study of the surface of a reference sample showed that it has (Fig. 4a)

- formed during machining grooves-scratches, microscopic irregularities and traces of plastic deformation with burrs and torn edges, which form the microrelief and, consequently, surface roughness, as well as pronounced areas of heat-affected zones.
- carbide phase precipitation in the form of globules of 1–5 microns average size irregularly distributed on the surface.

The surface of the sample treated in low-temperature plasma looks different (Fig. 4b). The edges of the burrs on it are melted, all the irregularities are smoothed out, there are no minor scratches. The carbide phase precipitation are less noticeable. The surface lightening indicates a change in its chemical composition as a result of the conversion of alloying elements that make up the carbide phase to a solid solution, which is possible only if it is dissolved (it is known that it occurs at a surface temperature of 1050–1110 °C, which corresponds to the amount of heat of ≈100 J). At the same time, the interaction of electrostatic and electromagnetic fields in the processing unit is accompanied by the formation of a powerful oscillating near-wall layer of negative space charge where electrons are accelerated to energies of the order of hundreds eV. The main result is the formation of a stream of charged particles which, due to collisions with the sample surface, transfer their kinetic energy to it causing the sample to heat up. The evaluations showed [5] that this leads to the release of energy in the sample several times greater than that required to melt the thin surface layer and dissolve the carbide phase in it. However, taking into account the fact that the processing time was 8 min, and most of it was spent on heating the sample, complete dissolution did not occur since it requires at least 15 min [10]. Thus, both individual unordered atoms and dense metastable groups of atoms with higher local stability and non-crystallographic ordering symmetry were present in the melt at the same time. Subsequent quenching under reduced pressure led to fixation (solidification) of the melt.

Microhardness test results showed that the sample processed in low-temperature plasma:

- microhardness in the layer at a depth of up to 2 microns doubled from 3.8 GPa to 7.6 GPa;
- the surface layer was more consolidated in comparison with the surface layer of the untreated sample, since, under the same load, the indenter penetrated to a smaller depth (Fig. 5);
- the greatest consolidation also occurred in the layer at a depth of up to 2 microns.

A more detailed study of the sample surface layer treated in a low-temperature plasma on a polished specimen established the following (Fig. 6):

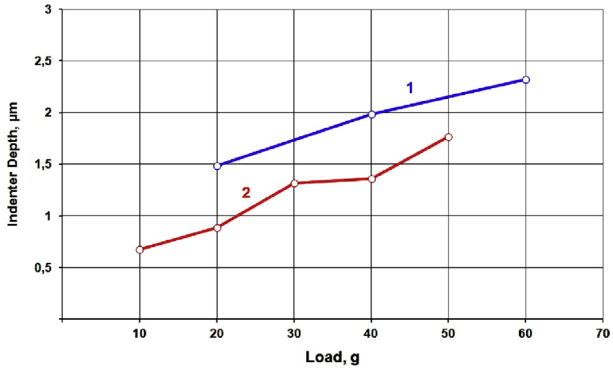

Fig. 5. Indentation depth variations in microhardness tests: 1 – reference sample, 2 – treated in low-temperature plasma.

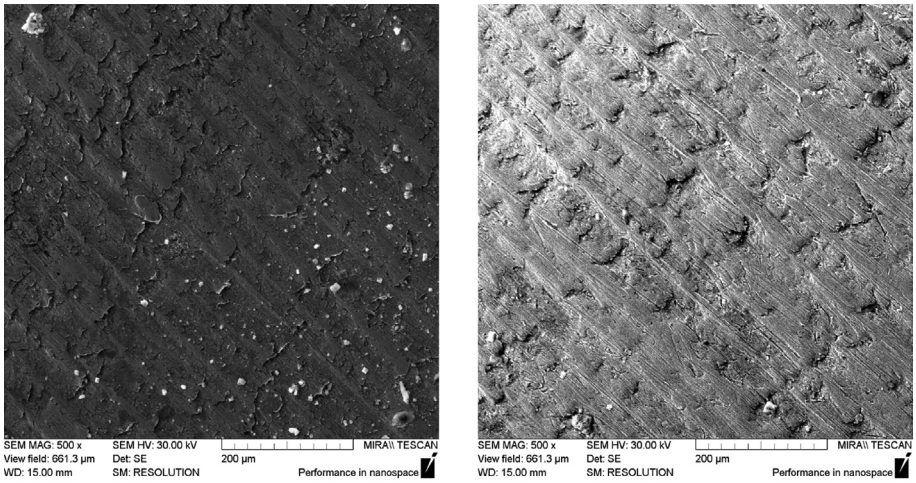

a b

Fig. 4. SEM images of sample surfaces prior corrosion tests: a – reference sample, b – treated in low-temperature plasma.

– near the boundary (at a depth of 1.5–2.0 μm) carbide phase globules have dimensions less than 0.5 μm (Fig. 6a);
– at a depth of more than 9.0 μm, the dimensions of carbide phase globules vary little compared with its dimensions in the core and are on the order of 1.0–1.5 μm (Fig. 6a);
– the core has a granular structure with inclusions of the carbide phase globules of 1.0–2.5 μm average sizes (Fig. 6b) in the nodes and along the boundaries;
– in the border regions of the section there is a 2 μm thick layer in which there are zones around the carbide phase globules containing numerous flat irregularly shaped particles of about 100 nm in thickness; they form a sphere/cloud (Fig. 6c) Outside this layer, the number of nanoscale particles is noticeably reduced. The presence of a meniscus on the surface of the globule in the region of its conjugation with the material, as well as nanosized particles separated from it (highlighted fragment in Fig. 6c) confirms the dissolution process as a result of heating the sample surface with low-temperature plasma and maximum consolidation of the near-surface layer.

The heating leads also to fusion of microroughness and to melt filling of hidden defects along the grain boundaries (Fig. 6d), i.e. their "healing", which improves the surface roughness.

It was also established that defects – steps, chips and cracks – are the centres of island film formation as a result of the adatom migration along the surface and surface diffusion. Film formation occurs under the condition that the energy of charged plasma particles (electrons and ions) entering the surface is below the potential barrier (Fig. 7). This leads to the adsorption and polymerization of carbon-containing radicals, the source of which are vapors of vacuum oil and neutral particles both in the gas phase and on the sample surface. The particle energy increase to a threshold value is accompanied by the film area extension as well as film density.

3.2. Results of corrosion test

The results determining corrosion losses are presented in Table 1 and show that the impact of low-temperature plasma led to the 3.17 times corrosion loss decrease, and 2.91 times corrosion rates decrease, i. e. a significant increase in corrosion resistance.

A study of the morphology and chemical composition of the sample surface layer showed that during the testing and according to the test results:

– corrosion processes in the reference sample proceeded at grain boundaries (Fig. 8a and c), whereas in a sample treated in low-temperature plasma they proceeded at the boundaries of the healed defects and in the amorphous bond (Fig. 8b and d);
– both the content of the main elements (Fig. 9), and their ratio in terms of reducing the amount of iron and chromium and increasing the amount of carbon and especially oxygen (Table 2) have changed.

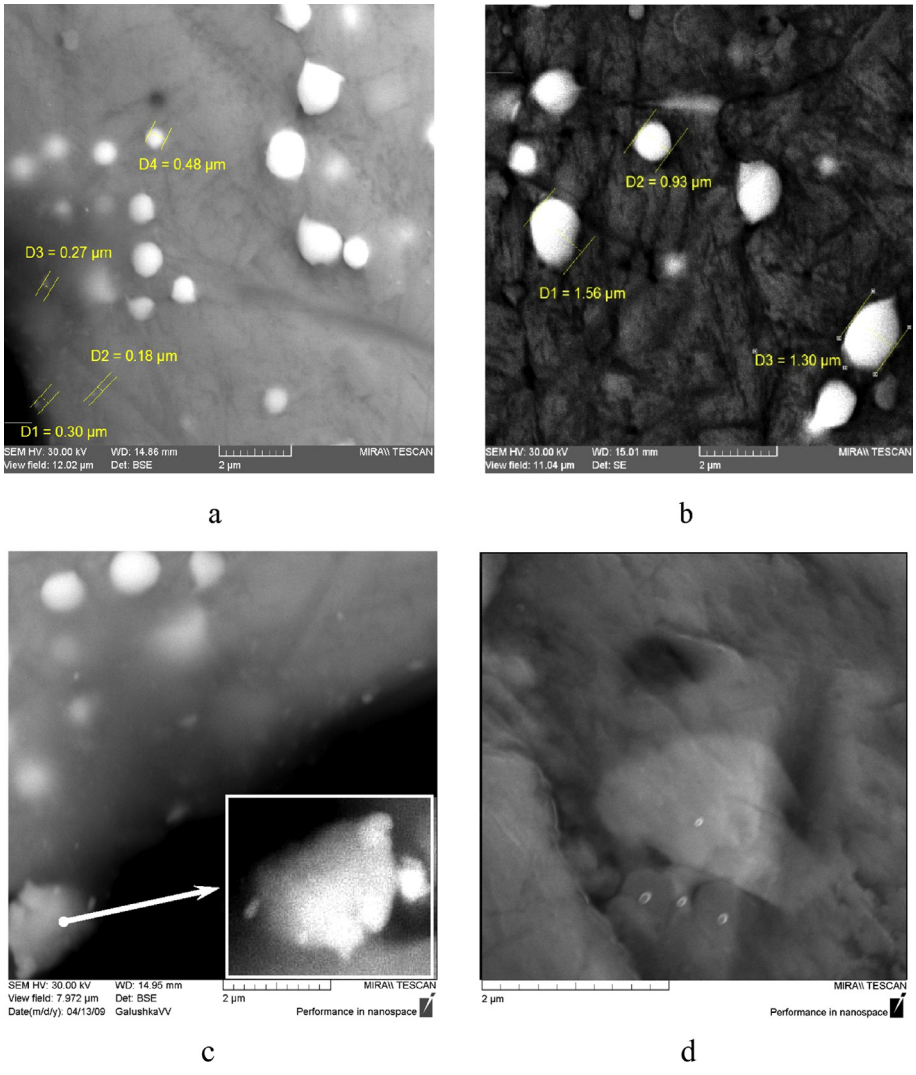

Fig. 6. Outcomes of the low-temperature plasma treatment.

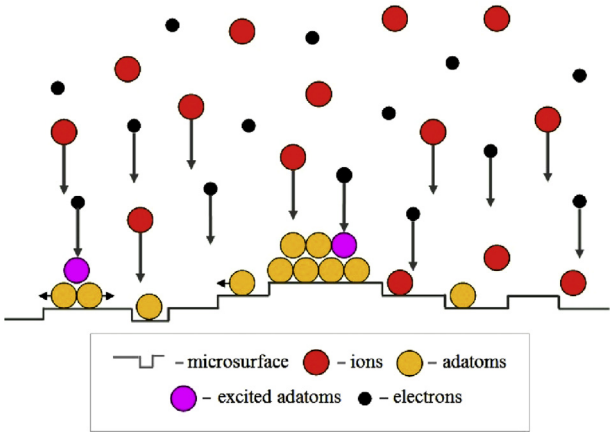

Fig. 7. The polymer film formation under the exposure of the sample surface to a compensated flow of charged plasma particles.

Table 1
Gravimetric corrosion test results.

Sample	Corrosion loss, g/square centimeter	Corrosion rate, g/(m^2×h)
Reference	0.0476	1.980
Low-temperature plasma treated	0.015	0.679

In this connection, it can be interesting to identify the mechanism underlying these results.

3.3. Identification of the surface passivation mechanism

It is known [11] that in a sodium chloride solution with a neutral reaction of the medium, steel corrosion proceeds via an electrochemical mechanism with oxygen depolarization. At the same time, in the areas of cementite which are cathodic sections in low-alloy steels, oxygen is restored in the steel structure:

$$O_2 + 4e + 2H_2O \rightarrow 4OH^-. \quad (2)$$

In addition, in the cathode region, oxygen compound formation occurs on the surface:

$$A(-): Fe^0 - 2e = Fe^{2+} \quad (3)$$

$$K(+): 2H2O + O2 + 4e = 4OH^- \quad (4)$$

$$2Fe^0 + 2H_2O + O_2 = 2Fe^{2+} + 4OH^- \quad (5)$$

$$2Fe^0 + 2H_2O + O_2 = 2Fe(OH)_2 \quad (6)$$

$$2Fe(OH)_2 + 1/2O_2 + H_2O = 2Fe(OH)_3 \quad (7)$$

$$2Fe(OH)_3 = Fe_2O_3 + H_2O \quad (8)$$

$$Fe(OH)_3 = FeOOH + H_2O \quad (9)$$

$$2Fe^0 + 2O_2 + 4H^+ \rightarrow 2FeO + 2H_2O \quad (10)$$

$$Fe^{2+} + H_2O \leftrightarrow Fe(OH)^+ + H^+ \quad (11)$$

$$4Fe^{2+} + O_2 + 6H_2O \leftrightarrow 4FeOOH + 8H^+. \quad (12)$$

Chloride ions serve as anodic corrosion stimulators due to adsorption on the surface and subsequent replacement of oxygen ions in the oxide

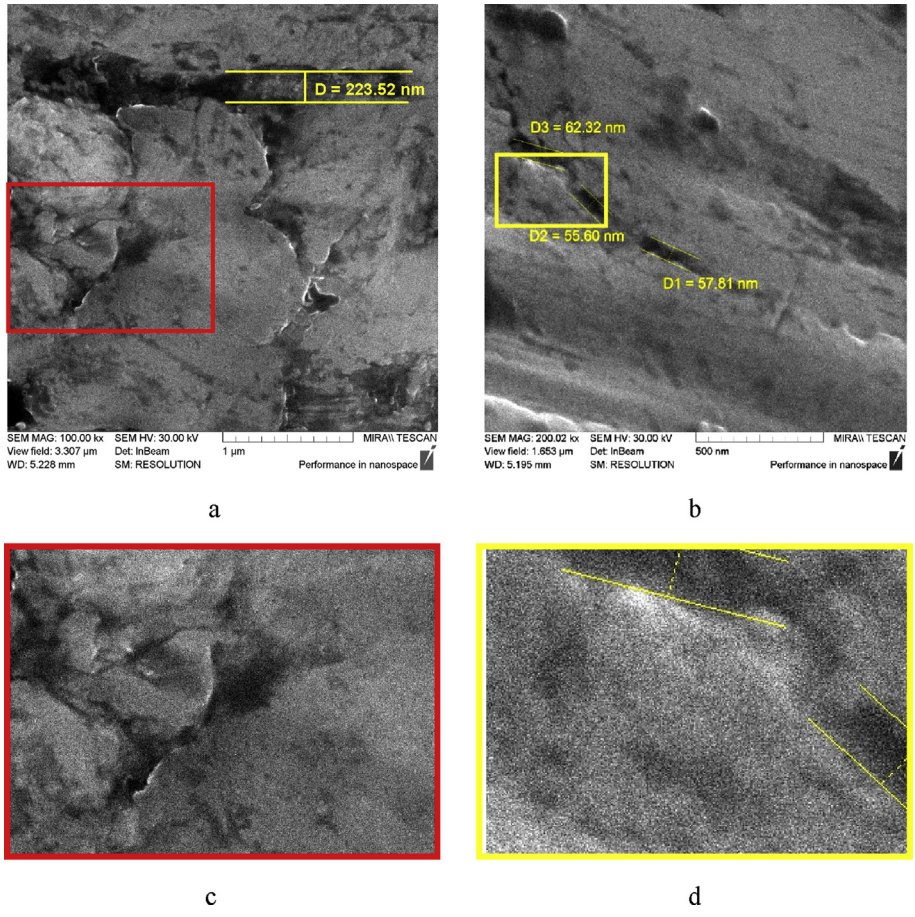

Fig. 8. SEM images of sample surfaces after corrosion tests: a – reference sample, b – treated in low-temperature plasma, c, d – highlighted fragment.

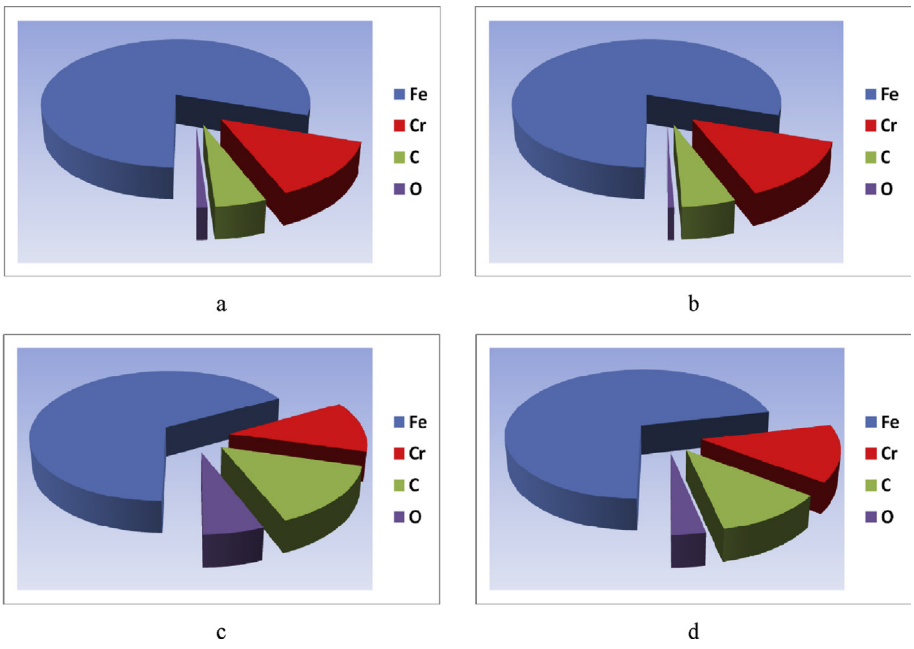

Fig. 9. The content of basic chemical elements in the surface layer before (a, b) and after (c, d) corrosion tests of the reference (a, c) sample and the low-temperature plasma treated sample (b, d).

Table 2
The main elements ratio in the sample surface layer.

No.	Unit	Reference sample	Plasma treated sample	Reference sample/plasma treated sample	
		Before and after testing		Before testing	After testing
		Content change relative to the initial,%		Content ratio, times	
1	Fe	16.2	10.6	1.0	0.9
2	Cr	11.7	1.9	1.0	0.9
3	C	-184.7*	-112.8*	1.0	1.3
4	O	-496.4*	-400.8*	1.5	1.8

* – content increase.

film. In the anode area, there occurs anodic dissolution of iron and chromium which ionize to the divalent state. At the same time, having a high tendency to passivation in oxidizing media, chromium is passivated, and its potential shifts from the standard one to the anode region, therefore, the formation of chromium compounds (IV) is possible:

$$Cr_2O_3 + H_20 - 2e^- = 2CrO_2 + 2H^+. \quad (13)$$

As a result, oxide and hydroxide layers are formed on the surface (or in the surface layer), which inhibit corrosion processes.

To test these findings using Raman spectroscopy, measurements were made of Raman scattering of sample surfaces, which is the inelastic scattering of optical radiation by molecules accompanied by a change in the substance frequency [12, 13, 14]. As a result, within the spectrum of scattered radiation there appear lines which are absent in the spectrum of the primary (excitation) light. Raman spectroscopy, being an informative non-destructive method, allows studying both the structure of various materials and its changes caused by different physical and/or chemical processes, since:

– the bands in the Raman spectra are a consequence of transitions between the vibrational levels of the atom, therefore only atoms that have chemical bonds with the surrounding atoms and are able to contribute to the scattering at a sufficient concentration contribute to the spectrum;
– dissolved atoms do not contribute to the spectrum.

The measurements and data processing showed (Fig. 10) that the surface spectra reflect the complex nature of Raman scattering and represent a superposition of absorption bands, which differ significantly from the spectrum of the initial surface. In the spectra of the reference sample both before and after the corrosion tests, wide and highly-overlapping bands of different intensity are observed. The spectrum of a plasma-treated sample after corrosion tests is characterized by a large number of narrower, slightly overlapping well-distinguishable bands.

The spectra were analyzed in two stages. At the first stage, they were compared with the known spectra of iron oxides and hydroxides: goethite (α-FeOOH) [12, 13, 14, 15, 16, 17, 18], acagenite (β-FeOOH) [12, 16, 19], lepidocrocite (γ-FeOOH) [12, 13, 14, 16, 17, 20], feoxyhite (δ-FeOOH) [12, 16], wüestite (FeO) [13, 16, 17], FeO_6 [21], hematite (α-Fe_2O_3) [12,13,16,17,22,23], maghemith (γ-Fe_2O_3) [12-14,16,23,24], magnetite (Fe_3O_4) [12,13,16,17,21,25-28], as well as chromium oxides: Cr_2O_3, CrO_2 [16,17,28,29] in the band of wave numbers 200-1200 cm^{-1}. These results made it possible to establish that the maximum difference in the intensities in the spectra of samples subjected to corrosion tests falls within the range of wave numbers 640-680 cm^{-1}. This range corresponds to phonon modes of symmetry A1g corresponding to optical transitions in iron ions. In this connection, in the second stage and within the indicated range, an index was calculated for each of the compounds which is the ratio of the intensities of the A1g vibrational modes (Table 3).

The analysis results made it possible to establish the following.

1. The intensity of the spectral bands of goethite, lepidocrocite, Feroxyhite, wüestite, hematite, maghemite, magnetite, CrO_2, FeO_6 in the reference sample is 7 ... 9 times higher than the intensity for the treated sample, which means blocking the oxygen ionization in a neutral solution, formation of oxides and hydroxides with the participation of electrons due to:
   – the appearance on the surface of new phases with properties of the diffusion barrier that prevents the convective transfer of OH^- ions from cathodic sections of the surface of the corrosive metal deep into the electrolyte;
   – increased density of near-surface layers;

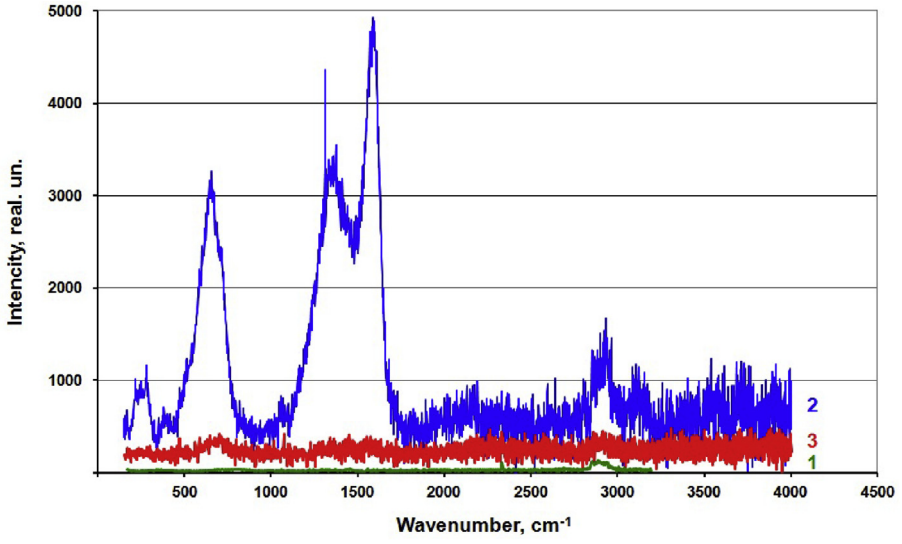

a

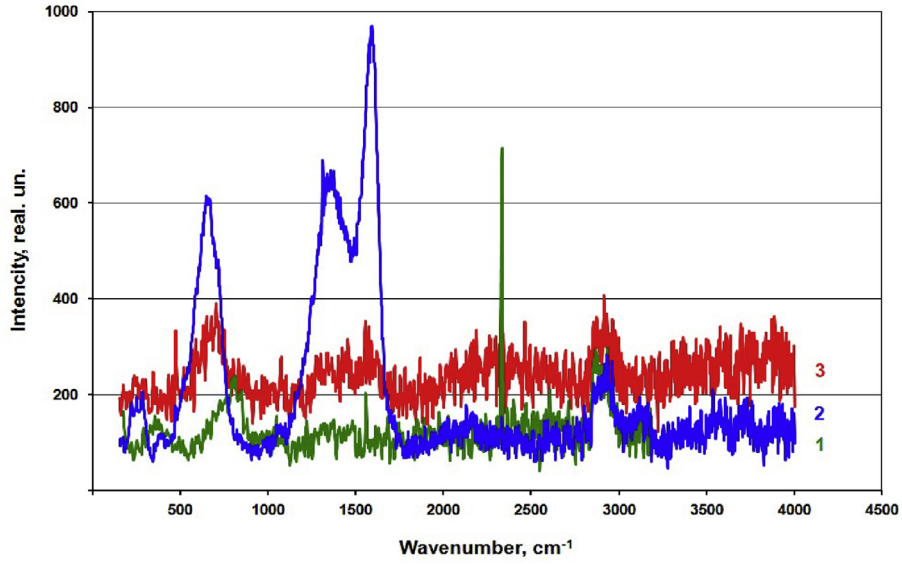

b

Fig. 10. The initial (a) and transformed (b) Raman spectra of sample surfaces: 1 – before corrosion tests; 2, 3 – reference and processed in low-temperature plasma after corrosion tests.

– "healing" of surface defects;
– reduction of the macrocathode area;
– increase of local electrical homogeneity of the surface.

As a result, the limiting stage of the oxygen depolarization shifts from diffusion to discharge-ionization, which leads to a decreased rate of oxides and hydroxides formation.

2. The intensity of the acagenite spectral bands in the reference sample exceeds the value of the intensity in the treated sample only by a factor of 4, which is associated with a 1.9 times increase, on average, in the rate of acagenite formation in the modified sample. In other words, amid the slowing down formation of oxides and hydroxides, the process of acagenite formation in the treated sample becomes dominant, taking course according to the following reactions [30]:

$$2FeCl_2 + 3H_2O + 1/2O_2 \leftrightarrow 2FeOOH + 4HCl; \quad (14)$$

$$2Fe + 4HCl + O_2 \leftrightarrow 2FeCl_2 + 2H_2O. \quad (15)$$

The release of hydrochloric acid which attacks iron unaffected by corrosion, leads to a continuous reproduction of ferric chloride $FeCl_2$ concentrated at the anode portions between the surface of metallic iron and its corrosion products, and, thereby, ensures the continuation of acagenite formation [31, 32].

The gradual accumulation of acagenite on the sample surface leads to the decrease in the rate of delivery of Cl^- anions to it, with the transition of the corrosion from the chemical to the diffusion stage which becomes its limiting stage.

Thus, the results of the analysis lead to the conclusion that the corrosion processes in the samples proceeded not only at different rates but also with various limiting stages (discharge-ionization and diffusion). The validity of this conclusion is confirmed by the fact that there is practically no correlation between the spectra (the correlation coefficient was 0.143).

Table 3
Results of Raman spectra analysis.

Compound	Sample	Parameters		
		Wave number, cm^{-1}	Intensity, rel. units	Intensity ratio
Goethite	Untreated	681.9	2645.8	7.80
	Treated	676.5	339.4	
Lepidocrocite	Untreated	651sh	3055	8.42
	Treated	649.3	363	
Acagenite	Untreated	671	2968.8	4.48
	Treated	674.7	663	
Feroxyhite	Untreated	681.9	2645	7.28
	Treated	676.5	363.2	
Wüestite	Untreated	649–651	3055.5	8.42
	Treated	649.3	363	
Hematite	Untreated	654.8	3058	8.42
	Treated	649.3	363.2	
Maghemith	Untreated	667.4	3036	9.27
	Treated	663.8	327.4	
Magnetite	Untreated	667	3036.7	9.29
	Treated	663	327	
Chromium Oxides	Untreated	660,2sh	3043	9.31
	Treated	663.8	327	

4. Conclusions

This work examines the effects of low-temperature combined-discharge plasma on the structure, physical and chemical properties of 40X13 steel using the gravimetric method, as well as scanning electron microscopy, Raman spectroscopy and microhardness tests. The results of the study can be summarized as follows:

(1) Low-temperature plasma, acting on the product for only 8 min:
- changes the surface layer chemical composition as a result of the conversion of alloying elements that make up the carbide phase into a solid solution;
- doubles the microhardness of the surface layer and consolidates it, most significantly at a depth of 2 μm;
- melts microroughness and "heals" latent defects along the grain boundaries, which contributes to the improvement of surface roughness;
- stimulates the island film formation as a result of the migration of adatoms along the surface and surface diffusion;
- has no significant effect on the core.

All of this enhances corrosion resistance due to 3.17 time reduction in corrosion losses and 2.91 time reduction of the corrosion rate.

(2) The improved corrosion resistance is based on:
- the blocking of oxygen depolarization as a result of the appearance of new phases with diffusion barrier properties, which leads to a change in the limiting stage of the formation of oxides and hydroxides of iron and chromium and, as a consequence, a decrease in the their formation rates.
- the decreased rate of delivery of Cl- anions to the surface, with the transition of corrosion from the chemical to the diffusion stage which becomes its limiting stage.

Declarations

Author contribution statement

B. Brzhozovskii: Conceived and designed the experiments; H. Zinina: Performed the experiments and interpreted the data; I. Gots: Performed the experiments and analized the data; M. Brovkova: Contributed reagents, materials analyses tools or data; V. Martynov: Discussed the results and wrote the paper.

Funding statement

This work was supported by The Russian Science Foundation.

Competing interest statement

The authors declare no conflict of interest.

Additional information

No additional information is available for this paper.

References

[1] I. Adamovich, S.D. Baalrud, A. Bogaerts, et al., the 2017 Plasma Roadmap: low temperature plasma science and technology, J. Phys. D: Appl. Phys. 50 (2017) 323001, 46pp.
[2] H.R. Maurer, H. Kersten, On the heating of nano- and microparticles in process plasmas, J. Phys. D: Appl. Phys. 44 (2011) 174029, 7pp.
[3] I. Lee, Effect of CH_4 content on the characteristics of surface layers of low temperature plasma nitrided 2205 Duplex stainless steel, Mater. Sci. Forum 879 (2016) 1074–1079.
[4] I. Lee, Effects of processing temperatures on the characteristics of the surface hardened layer produced on Duplex stainless steel by low temperature plasma nitrocarburizing, in: F. Marquis (Ed.), Proceedings of the 8th Pacific Rim International Congress on Advanced Materials and Processing, Springer, Cham, 2013, pp. 2025–2033.
[5] B. Brzhozovskii, M. Brovkova, S. Gestrin, V. Martynov, E. Zinina, The effect of a combined low-pressure gas discharge on metal surfaces, J. Phys. D: Appl. Phys. 51 (2018) 145204, 10pp.
[6] B. Brzhozovskii, V. Martynov, E. Zinina, M. Brovkova, Composite ion-plasma coatings with nanodisperse reinforced phase: scientific and practical aspects of synthesis, IOP Conf. Ser. Mater. Sci. Eng. 116 (2016), 012007.
[7] B. Brzhozovskii, V. Martynov, E. Zinina, M. Brovkova, Main problems and perspectives of the synthesis of nanocomposite coatings on the surface of complex-shaped components, IOP Conf. Ser. Mater. Sci. Eng. 116 (2016), 012008.
[8] A.D. MacDONALD, Microwave Breakdown in Gases, John Wiley & Sons Inc., New York – London – Sydney, 1966, p. 201.
[9] GOST 9.909-86, Unified system of corrosion and ageing protection. Metals, alloys, metal and non-metal inorganic coatings. Test Methods at Climatic Test Stations, M.: PKI standards Publishing, 1999, p. 13.
[10] G. Gottstein, Physical Foundations of Materials Science, Springer-Verlag, Berlin Heidelberg, 2004, p. 510.
[11] Herbert H. Uhlig, R. Winston Revie, Corrosion and Corrosion Control. An Introduction to Corrosion Science and Engineering, John Wiley & Sons, New York, 1985, p. 456.
[12] M.A. Legodi, Raman Spectroscopy Applied to Iron Oxide Pigments from Waste Materials and Earthenware Archaeological Objects, University of Pretoria, Pretoria, 2008, p. 106.
[13] M. Hanesch, Raman spectroscopy of iron oxides and (oxy)hydroxides at low laser power and possible applications in environmental magnetic studies, Geophys. J. Int. 177 (2009) 941–948.
[14] D.L.A. de Faria, S. Venaüncio Silva, M.T. de Oliveira, Raman microspectroscopy of some iron oxides and oxyhydroxides, J. Raman Spectrosc. 28 (1997) 873–878.
[15] A.A. Kompanchenko, A.V. Voloshin, M.Yu. Sidorov, Minerals of Fe in the oxidation zone of pyrite ores of the Yuzhno-Pechengskoj structural zone, Kola region: Raman spectroscopy identification, Bull. Moscow State Tech. Univ. 20 (1/1) (2017) 95–103.
[16] Colomban, P. Potential and Drawbacks of Raman (Micro)Spectrometry for the Understanding of Iron and Steel Corrosion. www.intechopen.com.
[17] Adar, F. Raman Spectra of Metal Oxides. Specy_WorkBench-FAdar-Raman_Spectra_of_Metal_Oxides-Oct_2014.
[18] Goethite R050142 - RRUFFID Database:Raman, X-ray, Infarend, and Chemistry.
[19] M. Szybowicz, M. Koralewski, J. Karo, L. Melnikova, Micro-Raman spectroscopy of natural and synthetic ferritins and their mimetics, Acta Phys. Pol., A 127 (2) (2015) 534–536.
[20] Lepidocrocite R050454 - RRUFFID Database:Raman, X-ray, Infarend, and Chemistry.
[21] Piotr Legutko, Tomasz Jakubek, Wojciech Kaspera, Paweł Stelmachowski, Zbigniew Sojka, Andrzej Kotarba, Strong enhancement of deSoot activity of transition metal oxides by alkali doping: additive effects of potassium and nitric oxide, Top. Catal. 60 (2017) 162–170.
[22] Hematite R050300 - RRUFFID Database: Raman, X-ray, Infarend, and Chemistry.
[23] L. Mazzetti, P.J. Thistlethwaite, Raman spectra and thermal transformations of ferrihydrite and schwertmannite, J. Raman Spectrosc. 33 (2002) 104–111.
[24] V.A. Vikulov, V.V. Balashev, T.A. Pisarenko, A.A. Dimitriev, V.V. Korobtsov, Thin magnetite films on an oxidized silicon surface: Raman spectroscopy study, Tech. Phys. Lett. 38 (8) (2012) 772–775.
[25] Š. Pešková, Vladimír Machovič, Petr Procházka, Raman spectroscopy structural study of fired concrete, Ceramics – Silikáty 55 (4) (2011) 410–417.
[26] Magnetite R080025 - RRUFFID Database:Raman, X-ray, Infarend, and Chemistry.

[27] Guilherme V.M. Jacintho, Alexandre G. Brolo, Paola Corio, Paulo A.Z. Suarez, Joel C. Rubim, Structural investigation of MFe2O4 (M = Fe, Co) magnetic fluids, J. Phys. Chem. C 113 (2009) 7684–7691.

[28] Brian D. Hosterman, Raman Spectroscopic Study of Solid Solution Spinel Oxides, Graduate College University of Nevada, Las Vegas, August 2011, p. 156. https://digitalscholarship.unlv.edu/thesesdissertations.

[29] V.P. Veiko, M.V. Yarchuk, A.I. Ivanov, Research of low-threshold mechanisms of modifying the structure of thin films of chromium under the influence of ultrashort laser pulses, Opt. Mag. 78 (8) (2011) 56–64.

[30] O.N. Tsybulskaya, I.Yu. Buravlev, A.A. Yudakov, A.Yu. Chirikov, Corrosion destructions of archaeological iron and methods of its stabilization, Bull. Far Eastern Branch Russian Acad. Sci. 5 (165) (2012) 23–31.

[31] Weijie Zhao, Ping Heng Tan, Jian Liu, Andrea C. Ferrari, Intercalation of few-layer graphite flakes with FeCl3: Raman determination of fermi level, layer by layer decoupling, and stability, J. Am. Chem. Soc. 133 (2011) 5941–5946.

[32] Melissa S. Sitze, Eric R. Schreiter, Eric V. Patterson, R. Griffith Freeman, Ionic liquids based on FeCl3 and FeCl2. Raman scattering and Ab initio calculations, Inorg. Chem. 40 (2001) 2298–2304.